PROCEEDINGS OF SCIENCE

# Production and properties of hypernuclei with ALICE

**Carolina Anna Jauch**[a,*] **for the ALICE collaboration**

[a] *Physikalisches Institut Universität Heidelberg, Im Neuenheimer Feld 226, Heidelberg, Germany*

*E-mail:* c.reetz@cern.ch

Hypernuclei are bound states of nucleons and hyperons. The measurement of the production of hypernuclei with mass numbers A = 3 and A = 4 in proton-proton and heavy-ion collisions is a powerful tool to investigate the hypernucleosynthesis mechanism. In the coalescence model, the production yields are sensitive to the interplay between the spatial extension of the nucleus wavefunction and the baryon-emitting source size, whereas, in the statistical hadronisation model, the nuclear structure does not come into play. Hypernuclei span a wide range of wavefunction radii, from about 2 fm for A = 4 hypernuclei to about 10 fm for the hypertriton, making them ideal probes to test such models in various collision systems. In addition, the study of hypernuclei properties provides information on nucleon-hyperon interactions, complementing the results obtained through femtoscopy correlation measurements. The strength of such interactions is a fundamental input to calculate the equation-of-state of the high-density nuclear matter found inside neutron stars. A precise understanding of the hypertriton decay modes and their branching ratios contributes to further constraining its properties. However, current experimental knowledge of them remains limited. This can be addressed through a measurement of its charged mesonic three-body decay into $\mathrm{d} + \mathrm{p} + \pi$, as presented in this contribution. Recent measurements of $^{3}_{\Lambda}\mathrm{H}$, $^{4}_{\Lambda}\mathrm{H}$, and $^{4}_{\Lambda}\mathrm{He}$ are reported, based on data samples collected by the ALICE experiment during LHC Run 2 and Run 3. The results are compared with predictions from state-of-the-art production models that implement both coalescence and thermal approaches.

PoS(EPS-HEP2025)199

*Speaker

© Copyright owned by the author(s) under the terms of the Creative Commons Attribution-NonCommercial-NoDerivatives 4.0 International License (CC BY-NC-ND 4.0).
All rights for text and data mining, AI training, and similar technologies for commercial purposes, are reserved.
ISSN 1824-8039. Published by SISSA Medialab.

https://pos.sissa.it/

## 1. Introduction

Hypernuclei are loosely bound states of nuclei and strange baryons (hyperons), which extend the nuclear chart by a third dimension, the strangeness one. Via the measurement of their properties like the lifetime and binding energy, hypernuclei serve as unique direct probes for the study of the interaction of hyperons with ordinary matter (Y–N). Theoretical models predict the production of hyperons to be favourable in the innermost core of neutron stars [1, 2], which results in a softening of their equation-of-state. However, this is in tension with the observation of various high mass neutron stars [3]. Several attempts have been made to solve this discrepancy. Models introducing additional three body repulsion interactions, Y–N–N, manage to describe the observed neutron star masses [2]. In order to constrain these models, a precise experimental knowledge of the Y–N and Y–N–N interactions is crucial. In addition to the approach of femtoscopic correlation measurements, the precise knowledge of the lifetime and binding energy of hypernuclei, which reflect the strength of the Y–N interaction, provides important experimental constraints.

Due to its shallow binding and large size, the hypertriton, ${}^{3}_{\Lambda}\mathrm{H}$, specifically is a sensitive probe for the nuclear production mechanism. The hypernucleosynthesis in hadronic collisions is currently modelled with two distinct approaches. The thermal models or statistical hadronisation models (SHM) [4] approach the particle production thermodynamically and predict that both hadrons and hypernuclei are emitted from a common interaction region which is in statistical equilibrium at the same chemical freeze-out temperature, $T_{\mathrm{ch}}$. These types of models are very successful in predicting the abundances of different particle species in hadronic collisions at the LHC, and for the moment do not exhibit any dependence on the structure of the produced hypernucleus [5]. The second approach describes hypernuclei formation via coalescence of nucleons and hyperons, which are close in phase space at the kinetic freeze-out of the system [6, 7]. The production probability via coalescence depends on the overlap of the nuclear wavefunction and the phase space of the nucleons. In contrast to the SHM approach, coalescence models incorporate the wavefunction of the created object.

## 2. ${}^{3}_{\Lambda}\mathrm{H}$ production in small collision systems

The ${}^{3}_{\Lambda}\mathrm{H}$ is the lightest known hypernucleus composed of a $\Lambda$ baryon, a proton, and a neutron. Its $\Lambda$ separation energy, $B_{\Lambda}$, of only a few hundred keV [9] translates into an extended wavefunction of about 10 fm [10]. Taking into account this very weakly bound nature of the ${}^{3}_{\Lambda}\mathrm{H}$, both production models discussed previously predict a suppression of its production in systems with small charged-particle multiplicity. The SHM is independent of the size of the produced object and predicts a suppression due to the canonical conservation of the quantum numbers in these small systems [8]. The coalescence model, on the other hand, is sensitive to the interplay between the collision system size and the spatial extension of the ${}^{3}_{\Lambda}\mathrm{H}$ wavefunction. Therefore, it predicts a suppressed ${}^{3}_{\Lambda}\mathrm{H}$ yield in small systems [7] with respect to the SHM expectation due to the decreased emission source size, which becomes small compared to the wide ${}^{3}_{\Lambda}\mathrm{H}$ wavefunction. The discrepancy between the two model predictions for the ${}^{3}_{\Lambda}\mathrm{H}$ production at low charged-particle multiplicities can be exploited to discriminate between the different hypernucleosynthesis mechanisms. A precise measurement of the integrated ${}^{3}_{\Lambda}\mathrm{H}$ yield measured in the two-body mesonic charged decay channel to ${}^{3}\mathrm{He} + \pi$ in pp



PoS(EPS-HEP2025)199

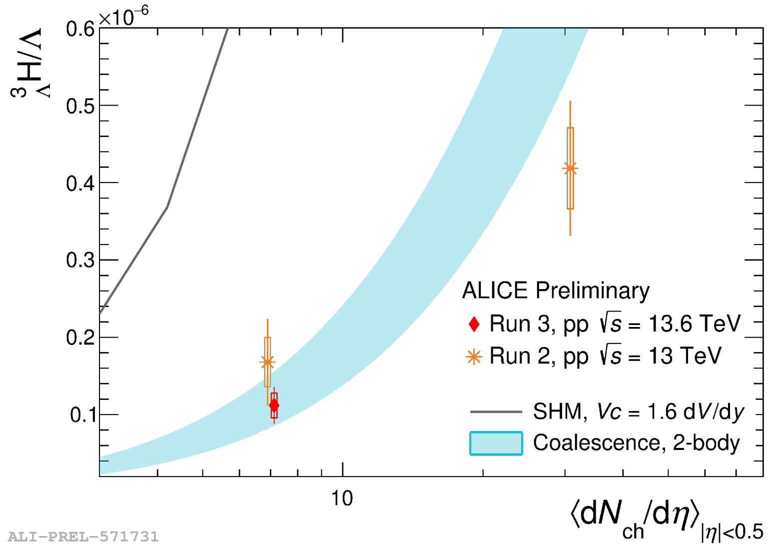


**Figure 1:** ${}^{3}_{\Lambda}\mathrm{H}/\Lambda$ yield ratio as a function of the average charged-particle multiplicity measured in Run 2 pp collisions at $\sqrt{s}$ = 13 TeV (orange markers) and Run 3 pp collisions at $\sqrt{s}$ = 13.6 TeV (red marker). Expectations from the SHM [8] and two-body coalescence model [7] are shown by the black solid line and the blue band, respectively.

collisions at $\sqrt{s}$ = 13.6 TeV with the ALICE detector presented in Fig. 1 shows a clear tension with the SHM prediction and sets a strong constraint on the model configuration. It is found that the coalescence picture is able to describe the measured ${}^{3}_{\Lambda}\mathrm{H}$ suppression in pp collisions which suggests that the nuclear size of the created object seems to matter at low charged-particle multiplicities.

### 2.1 ${}^{3}_{\Lambda}\overline{\mathrm{H}} \rightarrow {}^{3}\overline{\mathrm{He}} + \pi^{+}$ production measurement in pp collisions at $\sqrt{s}$ = 13.6 TeV

In the coalescence picture, the emission source size is reduced with increasing $p_{\mathrm{T}}$ of the ${}^{3}_{\Lambda}\mathrm{H}$, which leads to a suppression of its yield at high $p_{\mathrm{T}}$ [12]. The measurement of the $p_{\mathrm{T}}$-differential production cross section therefore allows to differentiate between thermal production and coalescence and to place constraints on the coalescence parameters and the ${}^{3}_{\Lambda}\mathrm{H}$ wavefunction. Figure 2 presents the $p_{\mathrm{T}}$-differential ${}^{3}_{\Lambda}\overline{\mathrm{H}}$ production cross section measured at midrapidity in pp collisions at $\sqrt{s}$ = 13.6 TeV with the ALICE detector. The measurement is compared to two predictions from the ToMCCA coalescence model [11], a coalescence afterburner which employs a realistic ${}^{3}_{\Lambda}\mathrm{H}$ wavefunction. It provides the first ever prediction for the ${}^{3}_{\Lambda}\mathrm{H}$ $p_{\mathrm{T}}$-spectrum. In this case, the measured spectrum is well described by the prediction employing a Congleton wavefunction for the ${}^{3}_{\Lambda}\overline{\mathrm{H}}$ shown by the red band.

### 2.2 ${}^{3}_{\Lambda}\mathrm{H} \rightarrow \mathrm{d} + \mathrm{p} + \pi$ reconstruction in pp collisions at $\sqrt{s}$ = 13.6 TeV

In recent years, precise measurements of the ${}^{3}_{\Lambda}\mathrm{H}$ binding energy and lifetime using the decay to ${}^{3}\mathrm{He} + \pi$ became feasible [9]. Direct experimental measurements of the ${}^{3}_{\Lambda}\mathrm{H}$ decay modes with their branching ratios, however, are still missing. From pionless effective field theory (EFT) calculations [13], where $B_{\Lambda}$ enters as a free parameter, it is found that the sum of the partial decay widths of the



PoS(EPS-HEP2025)199

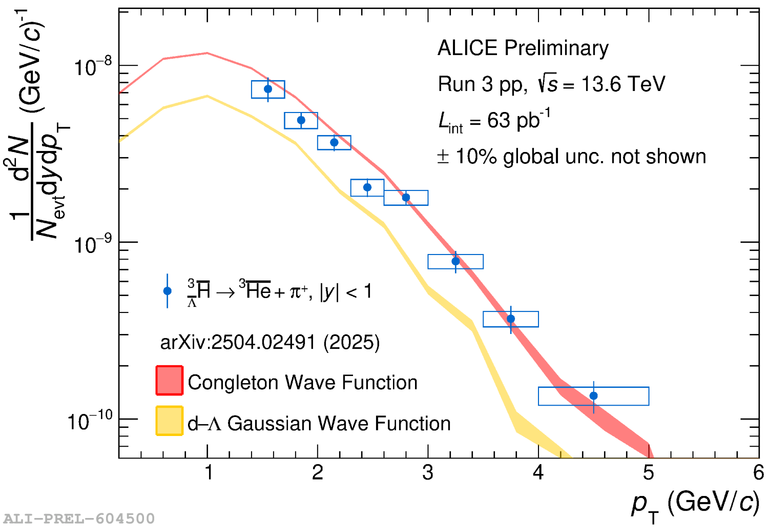


**Figure 2:** $^{3}_{\Lambda}\overline{\mathrm{H}} \rightarrow {}^{3}\overline{\mathrm{He}}{+}\pi^{+}$ spectrum measured at midrapidity in pp collisions at $\sqrt{s}$ = 13.6 TeV. Statistical and systematic measurement uncertainties are indicated as errorbars and boxes, respectively. The measurement is compared to the ToMCCA coalescence model [11] employing a Congleton wavefunction (red band) and a Gaussian wavefunction (yellow band) for the $^{3}_{\Lambda}$H.

dominant charged mesonic decays shows a strong dependence on the value of $B_{\Lambda}$ [13]. Specifically, a measurement of the production rates ratio R$_3$

$$\mathrm{R}_3 = \frac{\Gamma(^{3}_{\Lambda}\mathrm{H} \rightarrow {}^{3}\mathrm{He} + \pi)}{\Gamma(\mathrm{all}\,\pi^{-}\,\mathrm{decay\,channels})} \approx \frac{\Gamma(^{3}_{\Lambda}\mathrm{H} \rightarrow {}^{3}\mathrm{He} + \pi)}{\Gamma(^{3}_{\Lambda}\mathrm{H} \rightarrow {}^{3}\mathrm{He} + \pi) + \Gamma(^{3}_{\Lambda}\mathrm{H} \rightarrow \mathrm{d} + \mathrm{p} + \pi)} \tag{1}$$

can therefore provide an additional experimental constraint for the $^{3}_{\Lambda}$H properties. To achieve this, the $^{3}_{\Lambda}$H is reconstructed for the first time via its three-body decay into d + p + $\pi$ in pp collisions at $\sqrt{s}$ = 13.6 TeV with the ALICE detector at the LHC. The measured $^{3}_{\Lambda}$H invariant mass spectrum contains different background components which need to be modelled precisely in order to be able to extract the signal. Due to the low $Q$-value of the decay, the background exhibits a pronounced edge close to the expected mass of the $^{3}_{\Lambda}$H, caused by background from uncorrelated pairs of deuterons and $\Lambda$ baryons, which decayed into a proton and a $\pi$. Additionally, the background contains fully uncorrelated triplets of deuterons, protons, and $\pi$, as well as correlated $\Lambda$–d pairs. The latter are not specifically modelled in this analysis but will be addressed in a future detailed study using the decay topology. The individual background components are estimated using the event mixing technique. The corresponding mixed-event and same-event invariant mass spectra are presented in Fig. 3. The combination of a deuteron and $\pi$ from one event with a proton from another (mixed proton background) is used to estimate the fully uncorrelated background component. Pairing a proton and $\pi$ from one event with a deuteron from a second one (mixed deuteron background), on the other hand, gives an estimation for the total background consisting of the fully uncorrelated part and uncorrelated $\Lambda$–d pairs. The mixed-event invariant mass spectra shown in the left panels of Fig. 3 are used to constrain the background shape of the same-event candidate invariant mass spectrum presented in the right panel via a simultaneous fitting procedure. The successful reconstruction of



PoS(EPS-HEP2025)199

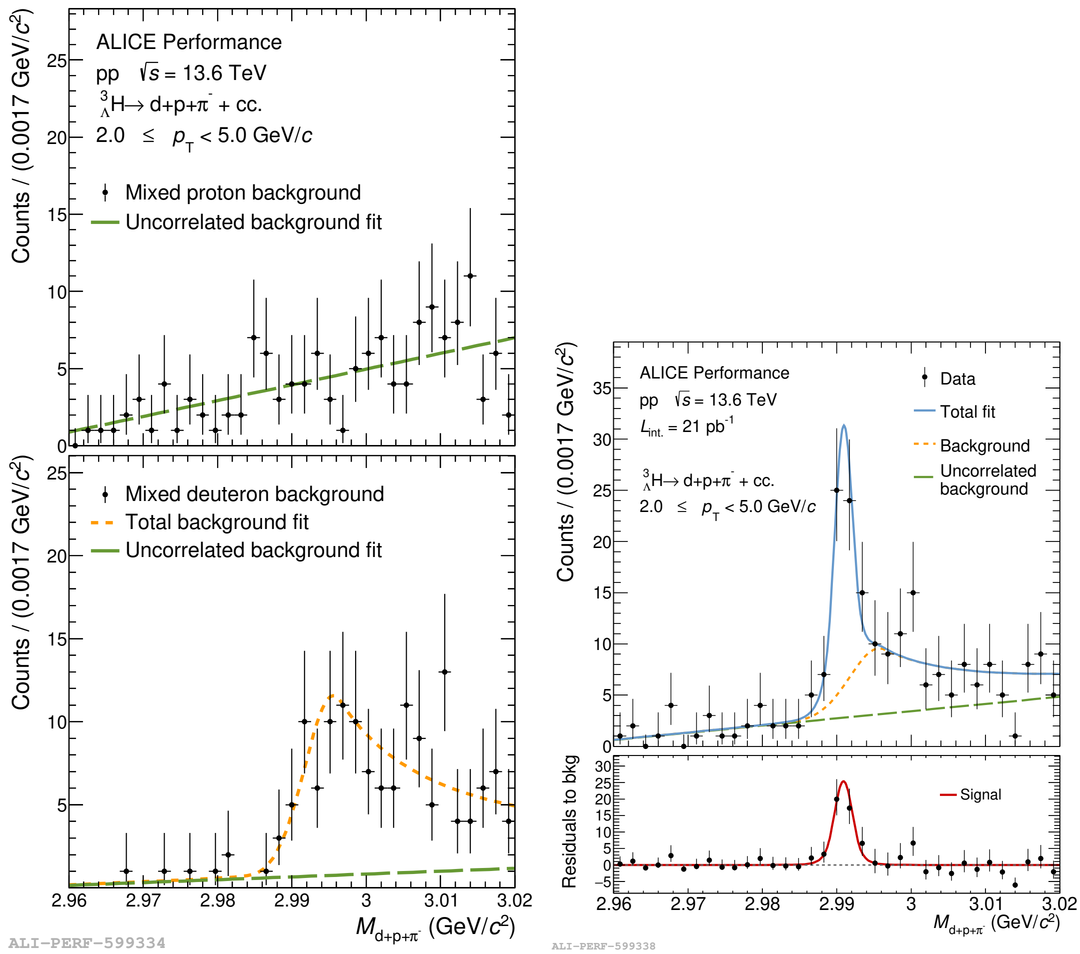


**Figure 3:** Mixed-event (left panels) and same-event (right panel) $d + p + \pi$ invariant mass spectra measured in pp collisions at $\sqrt{s}$ = 13.6 TeV at midrapidity with the ALICE detector.

the $^{3}_{\Lambda}\mathrm{H} \rightarrow d + p + \pi$ proves the feasibility of an $R_3$ measurement in Run 3 pp collisions with the ALICE detector at the LHC, which will help to further constrain the $^{3}_{\Lambda}$H properties.

### 2.3 Strangeness tracking for the reconstruction of $^{3}_{\Lambda}\mathrm{H} \rightarrow d + p + \pi$

The new ALICE Inner Tracking System (ITS2) consists of seven silicon layers based on Monolithic Active Pixel Sensors (MAPS) with the innermost layer placed close to the nominal interaction point at a distance of 22.4 mm [14]. It can be utilised to improve the three-body $^{3}_{\Lambda}$H decay vertex reconstruction via a direct detection of the $^{3}_{\Lambda}$H track in the silicon layers, which is combined with the vertex information from the traditional topological reconstruction from the weak decay daughter tracks. This new reconstruction technique called strangeness tracking improves the pointing resolution of the reconstructed candidate, quantified by the distance of closest approach (DCA) to the primary vertex of the collision, by a factor ~ 8. Furthermore, the background from Λ–d correlations is expected to be suppressed by the strangeness tracking technique, which is

PoS(EPS-HEP2025)199

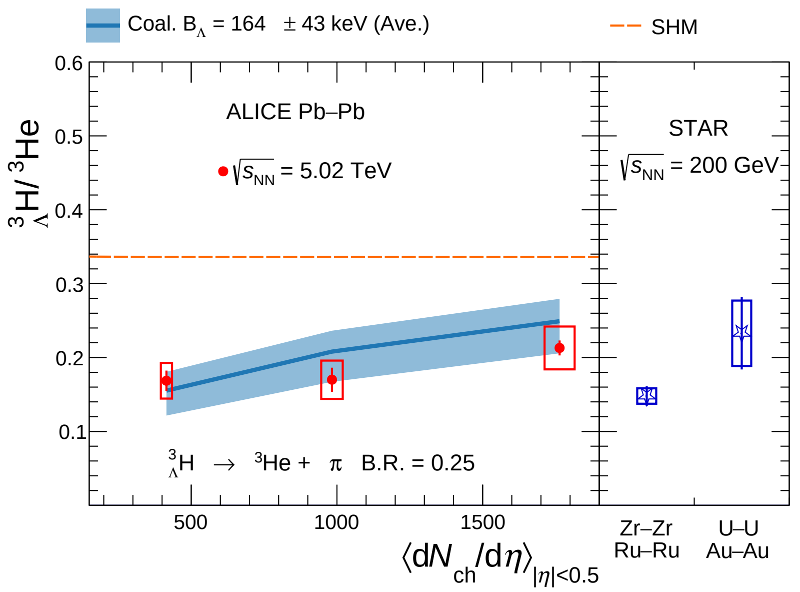


**Figure 4:** Yield ratio of $^{3}_{\Lambda}$H and $^{3}$He as function of multiplicity measured in Pb–Pb collisions at $\sqrt{s_{\rm NN}}$ = 5.02 TeV with ALICE (red markers). The result is compared to predictions from the SHM (orange dashed line) and the coalescence model (blue solid line with $1\sigma$ uncertainty band) [15].

therefore planned to be applied in the ongoing measurement of the $^{3}_{\Lambda}$H three-body decay using the pp collision data that are and will be recorded in the years 2025 and 2026.

## 3. $^{3}_{\Lambda}$H production in Pb–Pb collisions at $\sqrt{s_{\rm NN}}$ = 5.02 TeV

To further distinguish between different hypernucleosynthesis mechanisms, the $^{3}_{\Lambda}$H/$^{3}$He yield ratio is measured in Pb–Pb collisions at $\sqrt{s_{\rm NN}}$ = 5.02 TeV with the ALICE detector [15]. Figure 4 presents the result depending on the average charged-particle multiplicity of the system which reflects the size of the fireball. The expectation from the grand-canonical SHM (orange dashed line) is constant at the investigated large multiplicities and fails to capture the measurement. The coalescence model based on the Wigner function formalism [12] using the world average value for $B_\Lambda$ [16] predicts a suppression of the yield ratio for decreasing multiplicities due to the interplay between the decreasing emission source size and the wide $^{3}_{\Lambda}$H wavefunction. The measured $^{3}_{\Lambda}$H/$^{3}$He is well described by the presented coalescence prediction.

## 4. A = 4 hypernuclei in Pb–Pb collisions at $\sqrt{s_{\rm NN}}$ = 5.02 TeV

The more compact A = 4 hypernuclei have an increased Λ-separation energy compared to the $^{3}_{\Lambda}$H, which leads to the existence of excited states that decay electromagnetically into the ground state with lifetimes in the order of picoseconds [18, 19]. This feed-down from excited states contributes to the measured yield of the hypernuclei. By taking into account their spin degeneracy with a factor $2J + 1$, where $J$ is the spin of the considered state, the SHM computes the expected yield of the ground state and excited states separately [20, 21]. The comparison of these predictions to



PoS(EPS-HEP2025)199

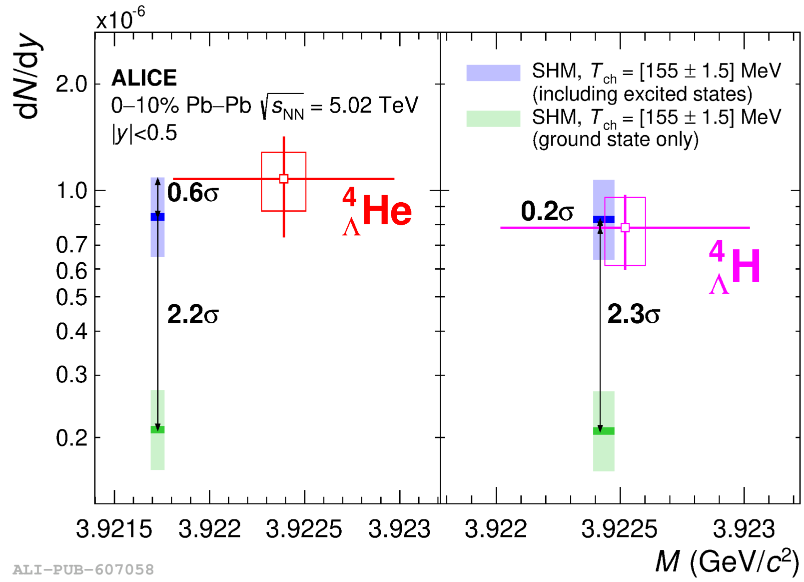


**Figure 5:** First measurement of the ${}^{4}_{\Lambda}$H (pink marker) and ${}^{4}_{\Lambda}$He (red marker) yields in central Pb–Pb collisions at $\sqrt{s_{\rm NN}}$ = 5.02 TeV at the LHC compared to SHM predictions considering only the ground states (green bands) or additionally including feed-down from excited states (blue bands) [17].

the measured yield of A = 4 hypernuclei could therefore provide information on the presence of excited states and test the production model dependence on the spin-degeneracy. Figure 5 presents the first measurement of the ${}^{4}_{\Lambda}$H and ${}^{4}_{\Lambda}$He yields at the LHC [17]. The results from central Pb–Pb collisions at $\sqrt{s_{\rm NN}}$ = 5.02 TeV recorded with the ALICE detector are compared to SHM predictions taking into account only the ground states of the measured hypernuclei (green bands), which show a clear deviation from the measured data. The inclusion of feed-down from excited states in the SHM (blue bands) enhances the expected yield by a factor $\sim$ 4 and leads to a good agreement with the measurements.

## 5. Summary and conclusions

The first $p_{\rm T}$-differential production cross-section measurement of ${}^{3}_{\bar{\Lambda}}\overline{\rm H}$ in pp collisions was presented. It was found to be well described by the advanced ToMCCA coalescence model employing a Congleton form for the ${}^{3}_{\Lambda}$H wavefunction. With the first successful reconstruction of ${}^{3}_{\Lambda}{\rm H} \rightarrow {\rm d} + {\rm p} + \pi$ in pp collisions with ALICE, it was demonstrated that the measurement of the production rates ratio will be feasible in LHC Run 3 data to eventually help constraining the ${}^{3}_{\Lambda}$H branching ratios and properties. While the measured suppression of the ${}^{3}_{\Lambda}{\rm H}/{}^{3}{\rm He}$ yield ratio with increasing charged-particle multiplicity in Pb–Pb collisions was found to be well described by a coalescence model prediction, it was not captured by the expectation from the grand-canonical SHM. However, the SHM prediction for A = 4 hypernuclei yields including feed-down from excited states is able to successfully describe the first measurement of these more compact objects at the LHC. The observables and methodologies presented in this contribution highlight the significant role of ALICE in constraining the production mechanisms, properties, and internal structure of various hypernuclei.



PoS(EPS-HEP2025)199

## References


[1] D. Logoteta, I. Vidaña, and I. Bombaci. "Impact of chiral hyperonic three-body forces on neutron stars". In: *Eur. Phys. J. A* 55 (2019), p. 207. DOI: 10.1140/epja/i2019-12909-9.

[2] D. Lonardoni et al. "Hyperon Puzzle: Hints from Quantum Monte Carlo Calculations". In: *Phys. Rev. Lett.* 114 (2015), p. 092301. DOI: 10.1103/PhysRevLett.114.092301.

[3] J. M. Lattimer and M. Prakash. "The Physics of Neutron Stars". In: *Science* 304.5670 (2004), pp. 536–542. DOI: 10.1126/science.1090720.

[4] A. Andronic et al. "Decoding the phase structure of QCD via particle production at high energy". In: *Nature* 561 (2018), pp. 321–330. DOI: 10.1038/s41586-018-0491-6.

[5] B. Dönigus. "Selected highlights of the production of light (anti-)(hyper-)nuclei in ultra-relativistic heavy-ion collisions". In: *Eur. Phys. J. A* 56 (2020), p. 280. DOI: 10.1140/epja/s10050-020-00275-w.

[6] S. T. Butler and C. A. Pearson. "Deuterons from High-Energy Proton Bombardment of Matter". In: *Phys. Rev.* 129 (1963), pp. 836–842. DOI: 10.1103/PhysRev.129.836.

[7] K.-J. Sun, C. M. Ko, and B. Dönigus. "Suppression of light nuclei production in collisions of small systems at the Large Hadron Collider". In: *Physics Letters B* 792 (2019), pp. 132–137. DOI: 10.1016/j.physletb.2019.03.033.

[8] V. Vovchenko, B. Dönigus, and H. Stoecker. "Multiplicity dependence of light nuclei production at LHC energies in the canonical statistical model". In: *Physics Letters B* 785 (2018), pp. 171–174. DOI: 10.1016/j.physletb.2018.08.041.

[9] S. Acharya et al. "Measurement of the Lifetime and $\Lambda$ Separation Energy of ${}^{3}_{\Lambda}\mathrm{H}$". In: *Phys. Rev. Lett.* 131 (2023), p. 102302. DOI: 10.1103/PhysRevLett.131.102302.

[10] F. Hildenbrand and H.-W. Hammer. "Three-body hypernuclei in pionless effective field theory". In: *Phys. Rev. C* 100 (2019), p. 034002. DOI: 10.1103/PhysRevC.100.034002.

[11] M. Mahlein et al. *ToMCCA-3: A realistic 3-body coalescence model*. 2025. arXiv: 2504.02491 [hep-ph].

[12] D.-N. Liu et al. "Softening of the hypertriton transverse momentum spectrum in heavy-ion collisions". In: *Physics Letters B* 855 (2024), p. 138855. DOI: 10.1016/j.physletb.2024.138855.

[13] F. Hildenbrand and H.-W. Hammer. "Lifetime of the hypertriton". In: *Phys. Rev. C* 102 (2020), p. 064002. DOI: 10.1103/PhysRevC.102.064002.

[14] B. Abelev et al. "Technical Design Report for the Upgrade of the ALICE Inner Tracking System". In: *Journal of Physics G: Nuclear and Particle Physics* 41.8 (2014), p. 087002. DOI: 10.1088/0954-3899/41/8/087002.

[15] S. Acharya et al. "Measurement of ${}^{3}_{\Lambda}\mathrm{H}$ production in Pb–Pb collisions at $\sqrt{s_{\mathrm{NN}}} = 5.02$ TeV". In: *Physics Letters B* 860 (2025), p. 139066. DOI: 10.1016/j.physletb.2024.139066.

[16] P. Eckert et al. *Chart of Hypernuclides — Hypernuclear Structure and Decay Data*. hypernuclei.kph.uni-mainz.de. 2023.




PoS(EPS-HEP2025)199

[17] S. Acharya et al. “First Measurement of $A = 4$ Hypernuclei and Antihypernuclei at the LHC”. In: *Phys. Rev. Lett.* 134 (2025), p. 162301. DOI: 10.1103/PhysRevLett.134.162301.

[18] M. Bedjidian et al. “Observation of a $\gamma$ transition in the $^{4}_{\Lambda}$H hypernucleus”. In: *Physics Letters B* 62.4 (1976), pp. 467–470. DOI: 10.1016/0370-2693(76)90686-9.

[19] T. O. Yamamoto et al. “Observation of Spin-Dependent Charge Symmetry Breaking in $\Lambda N$ Interaction: Gamma-Ray Spectroscopy of $^{4}_{\Lambda}$He”. In: *Phys. Rev. Lett.* 115 (2015), p. 222501. DOI: 10.1103/PhysRevLett.115.222501.

[20] B. Dönigus. “Hypernuclei at relativistic energies”. In: *EPJ Web Conf.* 276 (2023), p. 04002. DOI: 10.1051/epjconf/202327604002.

[21] V. Vovchenko et al. “Feeddown contributions from unstable nuclei in relativistic heavy-ion collisions”. In: *Physics Letters B* 809 (2020), p. 135746. DOI: 10.1016/j.physletb.2020.135746.

PoS(EPS-HEP2025)199